

# Parametrized Constant-Depth Quantum Neuron

Jonathan H. A. de Carvalho<sup>\*1</sup> and Fernando M. de Paula Neto<sup>1</sup>

<sup>1</sup>Centro de Informática, Universidade Federal de Pernambuco, Recife, Brazil  
{*jhac,fernando*}@*cin.ufpe.br*

## Abstract

Quantum computing has been revolutionizing the development of algorithms. However, only noisy intermediate-scale quantum devices are available currently, which imposes several restrictions on the circuit implementation of quantum algorithms. In this paper, we propose a framework that builds quantum neurons based on kernel machines, including on actual quantum devices. Previous schemes are particular cases of our generalized framework, where quantum neurons differ from each other by their feature space mappings. Under that framework, we present a neuron that applies a tensor-product feature mapping to an exponentially larger space. The proposed neuron is implemented by a circuit of constant depth with a linear number of elementary single-qubit gates. The existing neuron applies a phase-based feature mapping with an exponentially expensive circuit implementation, even using multi-qubit gates. Additionally, the proposed neuron has parameters that can change its activation function shape. Here, we show the activation function shape of each quantum neuron. It turns out that parametrization allows the proposed neuron to fit underlying patterns that the existing neuron cannot fit. As a result, the proposed neuron produces optimal solutions for the six classification problems addressed here, while the existing neuron only solves two of them. Finally, we demonstrate the feasibility of those quantum neuron solutions on a quantum

simulator.

## 1 Introduction

Quantum computing [1] is expected to achieve the so-called supremacy over classical computing, which will allow us to solve previously intractable problems in a reasonable time [2]. Specifically, that quantum advantage also allows the development of more efficient neural networks [3]. Quantum neurons can implement arbitrary non-linear functions while taking advantage of quantum properties like superposition and entanglement [4]. However, fault-tolerant quantum computations require encoding the information in many redundant qubits so that error correction codes can be employed [5].

Currently, only noisy intermediate-scale quantum devices are available, so there are not enough resources to protect the system by quantum error correction [6]. Depth, width, and number of operations become critical factors to successfully execute quantum circuits on the current hardware. Thus, aspects like state preparation, oracle expansion, connectivity, circuit rewriting, decoherence, gate infidelity, and measurement errors can compromise the computation [7].

Despite significant efforts at the quantum compiler level [8,9], recent quantum algorithms are developed considering those present restrictions [10,11], including the development of quantum neural networks [12–19]. Particularly, this work focuses on quantum perceptrons imple-

---

<sup>\*</sup>Corresponding author

mented efficiently on actual quantum devices. Tacchino et al. [12] took the first step by proposing a scheme that computes the inner product between binary-valued vectors. After, Mangini et al. [13] reformulated that scheme to accept continuous-valued vectors instead of only binary-valued ones. Both schemes have an exponential advantage in terms of circuit width, although the circuit depth and the number of operations grow exponentially.

In this work, we propose a framework of quantum neurons where those previous schemes [12, 13] are particular cases. Based on that framework, each quantum neuron implements a kernel machine with a non-deterministic activation function. That activation function depends only on the kernel trick each quantum neuron applies. Thus, the quantum neurons differ from each other by their feature space mappings. It makes room to instantiate other quantum neurons under that generalized framework, including for actual quantum devices.

Generally, quantum kernel methods are used to estimate inner products for classical models in a hybrid setup. The advantage emerges from the fact that the inner products are estimated from classically intractable feature mappings. Those inner products can be estimated by the standard swap-test [20] or, more recently, by quantum kernel estimators [21, 22]. Speedups in classical models can be also obtained by classical sampling techniques inspired by quantum models that generate the kernel matrix of inner products [23].

The framework of quantum neurons proposed here computes the inner product between an input vector and a weight vector, and then explicitly extracts such information to an ancillary qubit. Measuring the ancilla gives a standalone fully-quantum classifier based on kernel machines. If the ancilla is not measured, the inner product can be propagated forward to other quantum neurons, which gives a quantum neural network [14]. Finally, the proposed framework of quantum neurons is expected to achieve practical quantum advantage, as is expected with quan-

tum kernel estimators [24].

Based on that framework, we propose here a quantum neuron of constant depth, i.e., its circuit depth is independent of the input size. Constant-depth quantum circuits can demonstrate quantum advantage [25, 26] and benefit from error mitigation techniques [27–29]. The proposed quantum neuron implements local feature mappings [30] by taking advantage of qubit encoding [15, 19]. We demonstrate that encoding strategy actually implements a tensor-product feature mapping to an exponentially larger space, which improves the separating capacity [31].

We further improve that neuron capacity by including two parameters in its activation function. That parametrization can change the activation function shape of the proposed quantum neuron in order to fit different underlying patterns with no additional cost in the circuit implementation. Therefore, we propose a flexible quantum neuron of constant depth implemented with a linear number of elementary single-qubit gates. The existing quantum neuron [13] is inflexible and exponentially expensive, even with multi-qubit gates in its circuit implementation.

Then, we proceed to a visual study that relates some interactions between the input and weight vectors in the original space with the respective neuron outputs in the feature space. Those activation function shapes reveal the problem structures that each quantum neuron can solve. By comparing the best solutions of each quantum neuron for six classification problems, we show that parametrization can really change the activation function shape in order to fit underlying patterns that the existing quantum neuron cannot fit. The proposed quantum neuron produces optimal solutions for all six cases, which demonstrates its flexibility and improved capabilities. Finally, a proof-of-concept experiment on a quantum simulator demonstrates the feasibility of those quantum neuron solutions.

This paper is organized as follows. Firstly, Section 2 formalizes the quantum neuron framework based on kernel machines. The reader that

is not familiar with the basic concepts of quantum computing should refer to [1, 32]. Under the proposed framework, Section 3 presents the parametrized quantum neuron of constant circuit depth. The activation function shapes of the quantum neurons are presented in Section 4. Then, Section 5 compares the quantum neurons in solving some classification problems. Final remarks and future directions are discussed in Section 6.

## 2 Quantum Neuron Framework

The classical neuron model basically consists of two steps. First, the inner product between the input vector  $\vec{i}$  and the weight vector  $\vec{w}$  is computed, and then that inner product  $\sum_j w_j i_j$  is passed to an activation function  $\varphi(\cdot)$  in order to define the neuron output  $y$  [33]. Based on that model, one can construct different classical neurons by only changing the activation function that processes the obtained inner product. Examples of common activation functions are the Heaviside function and the logistic sigmoid function, which are presented in (1) and (2) respectively.

$$\varphi(\vec{w} \cdot \vec{i}) = \begin{cases} 1, & \text{if } \vec{w} \cdot \vec{i} \geq 0 \\ 0, & \text{if } \vec{w} \cdot \vec{i} < 0 \end{cases} \quad (1)$$

$$\varphi(\vec{w} \cdot \vec{i}) = \frac{1}{1 + e^{-(\vec{w} \cdot \vec{i})}} \quad (2)$$

Inspired by that classical neuron model, Tacchino et al. [12] proposed a scheme for actual quantum devices that encodes input and weight vectors, computes the inner product between them, and finally extracts the activation function output. Here, we generalize that scheme to a framework of quantum neurons based on kernel machines. Given two vectors  $\phi$  and  $\theta$  in an input space, a kernel machine  $k(\cdot, \cdot)$  maps those vectors to other two vectors  $\vec{w}$  and  $\vec{i}$  in a feature space by a nonlinear transformation  $\Phi(\cdot)$ , and then computes the inner product between the transformed

vectors, i.e.,  $k(\phi, \theta) = \Phi(\phi)^T \Phi(\theta) = \vec{w} \cdot \vec{i}$  [34]. The quantum neurons constructed by the framework are deeply related to that kernel trick, which paves the way to the quantum neuron that we propose in this work.

The quantum neurons implement kernel methods because the given  $m$ -dimensional classical vectors  $\theta$  and  $\phi$  are first mapped to  $N$ -dimensional quantum vectors  $\vec{i} = \Phi(\theta)$  and  $\vec{w} = \Phi(\phi)$ . Those quantum vectors can be directly encoded in legitimate quantum states in the following way:

$$|\psi_i\rangle = \sum_{j=0}^{N-1} i_j |j\rangle \quad \text{and} \quad |\psi_w\rangle = \sum_{j=0}^{N-1} w_j |j\rangle.$$

Then, the inner product  $\vec{w}^* \cdot \vec{i} = \langle \psi_w | \psi_i \rangle$  is computed by the quantum neurons. The final neuron output is given by the non-deterministic activation function presented in (3).

$$\varphi(\vec{w}^* \cdot \vec{i}) = \begin{cases} 1, & \text{with probability } |\vec{w}^* \cdot \vec{i}|^2 \\ 0, & \text{with probability } 1 - |\vec{w}^* \cdot \vec{i}|^2 \end{cases} \quad (3)$$

In this way, the quantum activation function depends on the inner product  $\vec{w}^* \cdot \vec{i}$  that in turn depends on the feature space mapping  $\Phi(\cdot)$ . Based on that framework, one can realize different quantum neurons, including on actual quantum computers, by only changing the mapping  $\Phi(\cdot)$  that each quantum neuron implements.

Figure 1 shows the circuit implementation of the framework of quantum neurons based on kernel machines. Specifically, the quantum neurons differ from each other by the quantum operators  $E$  and  $D$ , which depend on the classical vectors  $\theta$  and  $\phi$  respectively. The operator  $E$  maps  $\theta$  to  $\vec{i}$  and then encodes it in  $|\psi_i\rangle$  from  $|+\rangle^{\otimes n}$ , where  $|+\rangle = \frac{1}{\sqrt{2}}(|0\rangle + |1\rangle)$  and  $n$  is the number of encoding qubits. Thus,

$$E(\theta) |+\rangle^{\otimes n} = |\psi_i\rangle.$$

The operator  $D$  maps  $\phi$  to  $\vec{w}$  and then decodes it from  $|\psi_w\rangle$  to  $|+\rangle^{\otimes n}$ . Thus,

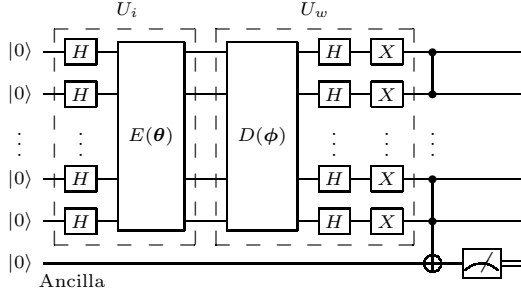


Figure 1: Framework circuit to build quantum neurons based on kernel machines. First,  $U_i$  encodes  $\vec{i} = \Phi(\theta)$ . Then,  $U_w$  computes the inner product between  $\vec{i}$  and  $\vec{w} = \Phi(\phi)$ . Such information is extracted to an ancillary qubit that gives a non-deterministic activation function when finally measured.

$$D(\phi) |\psi_w\rangle = |+\rangle^{\otimes n}.$$

At a higher level of abstraction, the operator  $U_i$  encodes  $|\psi_i\rangle$  from a blank register  $|0\rangle^{\otimes n}$ :

$$U_i |0\rangle^{\otimes n} = E(\theta) H^{\otimes n} |0\rangle^{\otimes n} = E(\theta) |+\rangle^{\otimes n} = |\psi_i\rangle.$$

On the other hand,  $U_w$  decodes  $|\psi_w\rangle$  to  $|1\rangle^{\otimes n}$ :

$$\begin{aligned} U_w |\psi_w\rangle &= X^{\otimes n} H^{\otimes n} D(\phi) |\psi_w\rangle = X^{\otimes n} H^{\otimes n} |+\rangle^{\otimes n} \\ &= X^{\otimes n} |0\rangle^{\otimes n} \\ &= |1\rangle^{\otimes n}. \end{aligned}$$

The operator  $D(\phi)$  and then  $U_w$  are defined according to the action on  $|\psi_w\rangle$ , but those operators are applied in  $|\psi_i\rangle$  in the circuit flow. Applying  $U_w$  to  $|\psi_i\rangle$  actually computes the inner product between  $\vec{i}$  and  $\vec{w}$  by taking advantage of an interesting property of unitary operators. Unitary operators preserve the space geometry, which includes inner products [32]. If  $A$  is a unitary operator, the inner product between a quantum state  $|v\rangle$  and another quantum state  $|v'\rangle$  is equal to the inner product between  $A|v\rangle$  and  $A|v'\rangle$ , i.e.,  $\langle v'|v\rangle = \langle v'A^\dagger|Av\rangle$ . Let  $A = U_w$ ,

$|v\rangle = |\psi_i\rangle$ , and  $|v'\rangle = |\psi_w\rangle$ . We can rewrite the expression as:

$$\langle \psi_w | \psi_i \rangle = \langle \psi_w U_w^\dagger | U_w \psi_i \rangle = \langle 1^{\otimes n} | U_w \psi_i \rangle.$$

Thus, the projection of  $U_w |\psi_i\rangle$  on the basis state  $|1\rangle^{\otimes n}$  stores the inner product  $\langle \psi_w | \psi_i \rangle$ . In other words, that inner product is stored in the component of  $|1\rangle^{\otimes n}$  into the superposition of  $U_w |\psi_i\rangle = |\psi_{i,w}\rangle$ . In this way,

$$\begin{aligned} |\psi_{i,w}\rangle &= c_0 |0\rangle + c_1 |1\rangle + \dots \\ &\quad + c_{N-2} |N-2\rangle + \langle \psi_w | \psi_i \rangle |N-1\rangle. \end{aligned}$$

To extract such information, a multi-controlled NOT gate is applied targeting an ancillary qubit. Note that only the basis state  $|N-1\rangle$  in the superposition flips the ancilla to the state  $|1\rangle$ . Consequently, the final quantum state  $|\psi_f\rangle$  is:

$$\begin{aligned} |\psi_f\rangle &= c_0 |0\rangle |0\rangle + c_1 |1\rangle |0\rangle + \dots \\ &\quad + c_{N-2} |N-2\rangle |0\rangle + \langle \psi_w | \psi_i \rangle |N-1\rangle |1\rangle. \end{aligned}$$

Since  $\langle \psi_w | \psi_i \rangle = \vec{w}^* \cdot \vec{i}$ , measuring that ancillary qubit finally gives the activation function already presented in (3). Therefore, that quantum neuron framework applies the kernel trick and activates following a non-deterministic function of the computed inner product, which was to be shown. To instantiate a quantum neuron, one only needs to realize a feature mapping  $\Phi(\cdot)$  by means of the operators  $E$  and  $D$ .

## 2.1 Binary-Valued Quantum Neuron

That generalized framework can be first instantiated in the binary-valued quantum neuron (BVQN) [12]. Given  $m$ -dimensional classical vectors  $\theta = (\theta_0, \theta_1, \dots, \theta_{m-2}, \theta_{m-1})$  and  $\phi = (\phi_0, \phi_1, \dots, \phi_{m-2}, \phi_{m-1})$ , where  $\theta_j, \phi_j \in \{-1, 1\}$ , the BVQN feature mapping simply normalizes those classical vectors, which leads to

the following  $N$ -dimensional quantum vectors, where  $N = m$ :

$$\vec{i} = \Phi(\boldsymbol{\theta}) = \frac{1}{\sqrt{N}} \left( \theta_0, \theta_1, \dots, \theta_{m-2}, \theta_{m-1} \right) \text{ and}$$

$$\vec{w} = \Phi(\boldsymbol{\phi}) = \frac{1}{\sqrt{N}} \left( \phi_0, \phi_1, \dots, \phi_{m-2}, \phi_{m-1} \right).$$

Those quantum vectors live in the Hilbert space spanned by  $n$  qubits, where  $N = 2^n$ . As  $N$  equals  $m$ , the BVQN has an exponential advantage in storing the information.

Note that  $|+\rangle^{\otimes n} = \frac{1}{\sqrt{N}} \sum_{j=0}^{N-1} |j\rangle$ , so  $E(\boldsymbol{\theta})$  only needs to flip the sign of the basis states  $|j\rangle$  where  $\theta_j = -1$  to encode  $\vec{i}$  in  $|\psi_i\rangle$ . Similarly,  $D(\boldsymbol{\phi})$  only needs to cancel the sign of the basis states  $|j\rangle$  where  $\phi_j = -1$  to decode  $\vec{w}$  from  $|\psi_w\rangle$ . Those operations are accomplished by applying sign-flip blocks one by one or, more efficiently, by applying the hypergraph states generation subroutine [12, 35]. However, those two strategies are exponentially expensive in terms of circuit depth. Finally, the BVQN fires with the probability presented in (4).

$$|\vec{w}^* \cdot \vec{i}|^2 = \left| \frac{1}{N} \sum_{j=0}^{m-1} \phi_j \theta_j \right|^2 \quad (4)$$

## 2.2 Continuous-Valued Quantum Neuron

A first alternative to accepting real vectors instead of only binary ones is to instantiate the framework in the continuous-valued quantum neuron (CVQN) [13], which implements a phase-based feature mapping. That mapping encodes each classical component in the phase of a complex number written in the exponential form with modulus  $1/\sqrt{N}$ . Thus, the classical vectors are mapped to quantum vectors of equal size in the following manner:

$$\vec{i} = \Phi(\boldsymbol{\theta}) = \frac{1}{\sqrt{N}} \left( e^{i\theta_0}, e^{i\theta_1}, \dots, e^{i\theta_{m-2}}, e^{i\theta_{m-1}} \right)$$

and

$$\vec{w} = \Phi(\boldsymbol{\phi}) = \frac{1}{\sqrt{N}} \left( e^{i\phi_0}, e^{i\phi_1}, \dots, e^{i\phi_{m-2}}, e^{i\phi_{m-1}} \right).$$

Periodicity in that phase-based scheme and the square modulus in the activation function make the CVQN equally recognize values that are actually different. To really distinguish such values, the classical vectors are scaled to the interval  $[0, \pi/2]$ . Thus, the feature mapping is applied to classical vectors  $\boldsymbol{\theta}$  and  $\boldsymbol{\phi}$ , where  $\theta_j, \phi_j \in [0, \pi/2]$ . The  $N$ -dimensional quantum vectors, where  $N = m$ , are described by  $n$  qubits, where  $N = 2^n$ , which represents an exponential advantage again in information storage.

To implement  $E(\boldsymbol{\theta})$  and  $D(\boldsymbol{\phi})$ , the blocks that flip the sign in the BVQN are used here to encode each  $e^{i\theta_j}$  and to decode each  $e^{i\phi_j}$ , respectively, by applying multi-controlled phase gates instead of multi-controlled  $Z$  gates. The phase gate  $P(\lambda)$  is represented in the matrix form by  $\begin{pmatrix} 1 & 0 \\ 0 & e^{i\lambda} \end{pmatrix}$ . As sign-flip blocks, phase-shift blocks are also exponentially expensive in terms of circuit depth. Finally, the CVQN fires with the probability presented in (5).

$$|\vec{w}^* \cdot \vec{i}|^2 = \left| \frac{1}{N} \sum_{j=0}^{m-1} e^{i(\theta_j - \phi_j)} \right|^2 \quad (5)$$

## 3 Proposed Quantum Neuron

Encoding data in the amplitudes of quantum states provides a gain in storage, but the circuit depth grows exponentially. Here, we propose to use a qubit encoding scheme under that framework of quantum neurons, differently from the BVQN and the CVQN that use amplitude encoding. In this way, an  $m$ -dimensional classical vector is encoded in  $m$  qubits, which represents less efficient storage, but the state preparation is definitely efficient in terms of circuit depth as each qubit only requires a single rotation to encode the data [15, 19]. That efficiency of qubit

encoding allows us to propose the constant-depth quantum neuron (CDQN).

Instead of a qubit encoding from rotations about the y-axis [15, 19], we apply that phase shift gate  $P(\lambda)$  already used in amplitude encoding previously [13]. Thus, the classical input vector  $\theta$  is directly encoded by the operator  $E$  as follows:

$$E(\theta) = \otimes_{j=0}^{m-1} P(\theta_j).$$

Similarly, the classical weight vector  $\phi$  is directly decoded by the operator  $D$  in the following way:

$$D(\phi) = \otimes_{j=0}^{m-1} P(-\phi_j).$$

As a result,  $U_i$  comes down to:

$$U_i = \otimes_{j=0}^{m-1} P(\theta_j) H^{\otimes m}.$$

In turn,  $U_w$  comes down to:

$$U_w = X^{\otimes m} H^{\otimes m} \otimes_{j=0}^{m-1} P(-\phi_j).$$

Therefore, with a circuit depth independent of the input size, the proposed quantum neuron computes the inner product between two vectors that are transformed by a tensor product of local feature mappings [30]. Those classical vectors are also pre-processed to the interval  $[0, \pi/2]$ , as for the CVQN.

Applying that  $E(\theta)$  in a basis state  $|s\rangle$  produces the following state:

$$E(\theta) |s\rangle = \prod_{j=0}^{m-1} (e^{i\theta_j})^{b_{j,s,m}} |s\rangle,$$

where  $b_{j,s,m}$  is the  $j$ -th bit in the binary representation of the integer value  $s$  with  $m$  bits. In this way,  $b_{j,s,m}$  selects the phase shifts to be applied. For example, with  $m = 4$ , applying  $E(\theta)$  in  $|5\rangle$  produces  $e^{i\theta_1} e^{i\theta_3} |5\rangle$ , using the big-endian convention. Applying  $E(\theta)$  in  $|+\rangle^{\otimes m}$  stores a conditioned product of  $e^{i\theta_j}$  on the amplitude of each possible state  $|s\rangle$ , which represents the following feature mapping, where  $N = 2^m$ :

$$\vec{i} = \Phi(\theta) = \frac{1}{\sqrt{N}} \left( \prod_{j=0}^{m-1} (e^{i\theta_j})^{b_{j,0,m}}, \prod_{j=0}^{m-1} (e^{i\theta_j})^{b_{j,1,m}}, \dots, \prod_{j=0}^{m-1} (e^{i\theta_j})^{b_{j,N-2,m}}, \prod_{j=0}^{m-1} (e^{i\theta_j})^{b_{j,N-1,m}} \right)$$

and

$$\vec{w} = \Phi(\phi) = \frac{1}{\sqrt{N}} \left( \prod_{j=0}^{m-1} (e^{i\phi_j})^{b_{j,0,m}}, \prod_{j=0}^{m-1} (e^{i\phi_j})^{b_{j,1,m}}, \dots, \prod_{j=0}^{m-1} (e^{i\phi_j})^{b_{j,N-2,m}}, \prod_{j=0}^{m-1} (e^{i\phi_j})^{b_{j,N-1,m}} \right).$$

Different from the previous quantum neurons, the CDQN maps  $m$ -dimensional classical vectors to  $N$ -dimensional quantum vectors with  $N > m$ . Specifically, the CDQN maps the vectors to an exponentially larger space. Thus, the CDQN is a kernel method that takes advantage of Cover's theorem [31], which states that mapping to feature spaces of high dimensionality improves the separating capacity. Non-linearly separable problems are more likely to become linearly separable in a high-dimensional space. Finally, the CDQN fires with the probability presented in (6).

$$|\vec{w}^* \cdot \vec{i}|^2 = \left| \frac{1}{N} \sum_{s=0}^{N-1} \prod_{j=0}^{m-1} (e^{i(\theta_j - \phi_j)})^{b_{j,s,m}} \right|^2 \quad (6)$$

We can simplify the relation presented in (6) by observing that it is actually a combination of  $m$  local inner products. Each local inner product is computed with respect to a local feature mapping that maps a  $\theta_j$  to  $\vec{i}_j = \frac{1}{\sqrt{2}}(1, e^{i\theta_j})$  and a  $\phi_j$  to  $\vec{w}_j = \frac{1}{\sqrt{2}}(1, e^{i\phi_j})$ . As a result, the relation presented in (6) is equivalent to a

product of  $m$  local inner products in the form  $\vec{w}_j^* \cdot \vec{i}_j = \frac{1}{2}(1 + e^{i(\theta_j - \phi_j)})$ . Therefore, the CDQN fires with a probability that can be simplified as presented in (7).

$$|\vec{w}^* \cdot \vec{i}|^2 = \left| \frac{1}{N} \prod_{j=0}^{m-1} (1 + e^{i(\theta_j - \phi_j)}) \right|^2 \quad (7)$$

Building on the CDQN, we also propose to parametrize its activation function by a multiplicative factor  $\tau$  and an additive constant  $\delta$ . Those parameters act on the component-wise differences between the classical input and weight vectors. In this way, the parametrized constant-depth quantum neuron (PCDQN) fires with the probability presented in (8). By adjusting  $\tau$  and  $\delta$ , the PCDQN can change its activation function shape. Thus, that parametrization generates flexibility. Such flexibility is supposed to allow the PCDQN to fit different underlying patterns.

$$|\vec{w}^* \cdot \vec{i}|^2 = \left| \frac{1}{N} \prod_{j=0}^{m-1} (1 + e^{i[\tau(\theta_j - \phi_j) + \delta]}) \right|^2 \quad (8)$$

At the circuit level, that parametrization is achieved by passing  $\tau\theta$  as the argument of  $E(\cdot)$  and  $\tau\phi$  as the argument of  $D(\cdot)$  followed by applying  $P(\delta)$  to each qubit. Figure 2 shows the circuit implementation of the PCDQN. As can be seen, the PCDQN is implemented by a circuit of constant depth with a linear number of elementary single-qubit gates. The PCDQN is not only efficient but also flexible due to  $\tau$  and  $\delta$ .

The PCDQN can be even more efficient by applying only one phase gate  $P(\lambda)$  to each qubit, where  $\lambda = \tau(\theta_j - \phi_j) + \delta$ . Therefore, the parametrization can be achieved with no additional cost in the circuit. However, the circuit presented in Figure 2 increases the depth by 1 and the number of operations by  $m$  to implement the parametrization.

To demonstrate the efficiency of the CDQN and the PCDQN over the CVQN, Figure 3 compares the circuit growth of each quantum neuron

as the input size increases. Figure 3a compares in terms of circuit depth and Figure 3b compares in terms of number of operations by using, respectively, the *depth* and *size* functions provided by Qiskit [36]. The blue curve represents the CVQN, the orange curve represents the CDQN, and the green curve represents the PCDQN.

As can be seen, the CVQN grows linearly with the input size  $m$  in terms of depth and number of operations. Since  $m = 2^n$  for the CVQN, that quantum neuron grows exponentially with the number of qubits  $n$ . On the other hand, the CDQN and the PCDQN have a constant depth and a lower number of operations. Additionally, the CDQN and the PCDQN are efficiently implemented with elementary single-qubit gates only, while the CVQN is expensive, even using complex phase-shift blocks.

## 4 Activation Function Shapes

Classical neuron outputs depend on some interaction between the input and weight vectors. For example, the larger the inner product between the vectors, the larger the output of the sigmoid activation function. As another example, the larger the Euclidean distance between the vectors, the smaller the output of the radial basis activation function. On the other hand, the quantum neuron outputs depend on the inner product between the input and weight vectors in the feature space. In this work, we study the quantum neuron outputs as a function of some relations between the original vectors, which can be seen as an indirect way to visualize quantum activation shapes.

Then, we defined a set of two-dimensional input vectors by splitting the interval  $[0, \pi/2]$  into ten equidistant values and taking all possible combinations, which gives an input set of one hundred vectors. The weight vector is fixed here as  $(\pi/2, \pi/2)$ . Thus, we compute the classical relations and the corresponding quantum neuron outputs for each input vector with respect

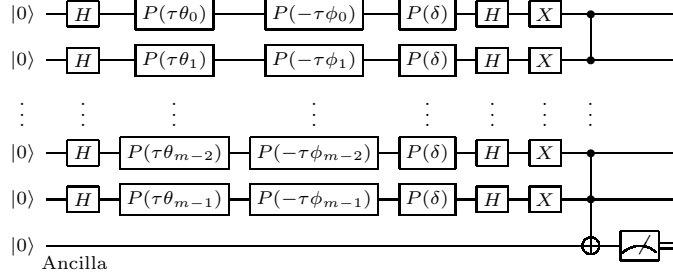


Figure 2: Circuit implementation of the PCDQN. Qubit encoding provides a constant-depth circuit with a linear number of elementary single-qubit gates. Additionally, the parameters  $\tau$  and  $\delta$  can change the PCDQN activation function shape.

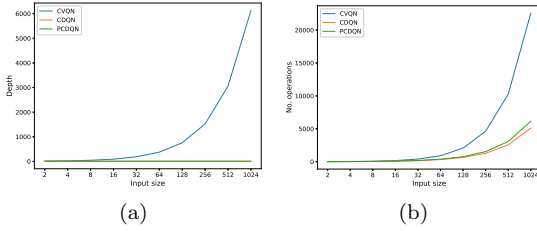


Figure 3: Circuit growth of each quantum neuron as the input size increases. The blue, orange, and green curves represent the CVQN, the CDQN, and the PCDQN growths, respectively. (a) in terms of circuit depth. (b) in terms of the number of operations.

to that weight vector of reference. Input vectors that give the same measure to that reference vector do not necessarily give the same neuron outputs. Specifically, we considered the following metrics provided by scikit-learn [37]: Manhattan distance, Euclidean distance, linear kernel, polynomial kernel, RBF kernel, and sigmoid kernel.

Figure 4 contrasts the CVQN activation with the CDQN activation as functions of the Manhattan distance, the Euclidean distance, and the linear kernel. The CVQN activation presents the same qualitative behavior in all cases but with a shift to the right for the Euclidean distance, as can be seen in Figure 4a, Figure 4b, and Figure 4c. In all cases, high values of activation are generated for the input vectors with extreme

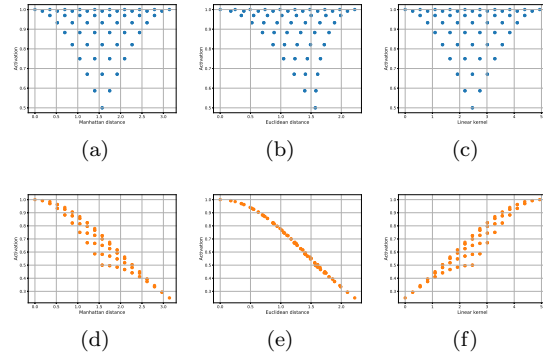


Figure 4: Quantum neuron activation as a function of the Manhattan distance, the Euclidean distance, and the linear kernel between the original input and weight vectors. (a), (b), and (c) for the CVQN. (d), (e), and (f) for the CDQN.

measures. Moving away from the extremes, the measures generate smaller and smaller values of activation in addition to the previous high values. Regarding the CDQN, its activation monotonically decreases as the Manhattan and Euclidean distances increase, as shown in Figure 4d and Figure 4e, and monotonically increases as the linear kernel also increases, as shown in Figure 4f.

In a similar way, Figure 5 contrasts the CVQN activation with the CDQN activation as functions of the polynomial kernel, the RBF kernel, and the sigmoid kernel. The CVQN activation



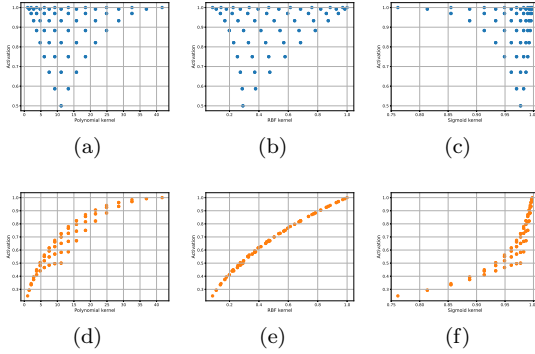


Figure 5: Quantum neuron activation as a function of the polynomial kernel, the RBF kernel, and the sigmoid kernel between the original input and weight vectors. (a), (b), and (c) for the CVQN. (d), (e), and (f) for the CDQN.

presents relatively the same qualitative behavior already presented in Figure 4 but with a shift to the left for the polynomial and RBF kernels, as shown in Figure 5a and Figure 5b, and a considerable shift to the right for the sigmoid kernel, as shown in Figure 5c. The CDQN activation presents relatively the same qualitative behavior already presented in Figure 4f but with shapes that suggest a logarithmic growth in Figure 5d, a linear growth in Figure 5e, and an exponential growth in Figure 5f.

Therefore, the CVQN and the CDQN can solve classification problems where those activation shapes fit correctly. It turns out the nature of each quantum neuron is preserved for any of those metrics. Thus, we follow the analysis in this work using only the Euclidean distance due to its intuitiveness.

Figure 6 shows the PCDQN activation as a function of the Euclidean distance for some combinations of  $\tau$  and  $\delta$ , which gives examples of substantial changes that are achieved by means of parametrization on that linear decay already presented in Figure 4e. For example,  $(\tau = 1/4, \delta = \pi/2)$  and  $(\tau = 1/2, \delta = \pi/4)$  give approximately a linear growth and a logarithmic growth, as shown in Figure 6a and Figure 6b.

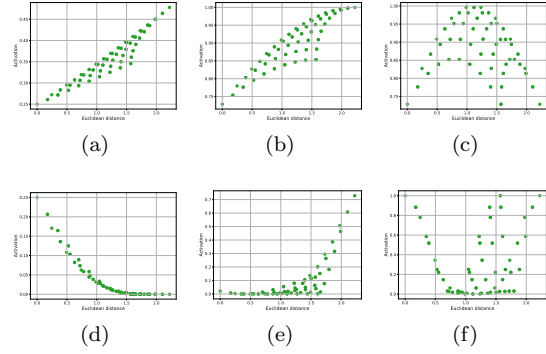


Figure 6: PCDQN activation as a function of the Euclidean distance between the original input and weight vectors for some combinations of  $\tau$  and  $\delta$ . (a) for  $\tau = 1/4$  and  $\delta = \pi/2$ . (b) for  $\tau = 1/2$  and  $\delta = \pi/4$ . (c) for  $\tau = 1$  and  $\delta = \pi/4$ . (d) for  $\tau = 1$  and  $\delta = 3\pi/2$ . (e) for  $\tau = 2$  and  $\delta = 5\pi/4$ . (f) for  $\tau = 4$  and  $\delta = 0$ .

Figure 6c shows a chain of concave-down parabolas achieved by  $(\tau = 1, \delta = \pi/4)$ . An exponential decay and an exponential growth are achieved by  $(\tau = 1, \delta = 3\pi/2)$  and  $(\tau = 2, \delta = 5\pi/4)$  respectively, as shown in Figure 6d and Figure 6e. Figure 6f approaches multiple concave-up parabolas with  $(\tau = 4, \delta = 0)$ . In summary, the PCDQN is flexible. In practice, such flexibility is expected to enable the PCDQN to fit problems that the other neurons cannot fit correctly.

## 5 Application on Classification Problems

Here, we numerically compare the quantum neurons at solving some classification problems. Additionally, we study the best solutions of the quantum neurons by means of their activation function shapes applied in the problems. Finally, we demonstrate the feasibility of those numerical solutions by executing the quantum neuron circuits on a quantum simulator.

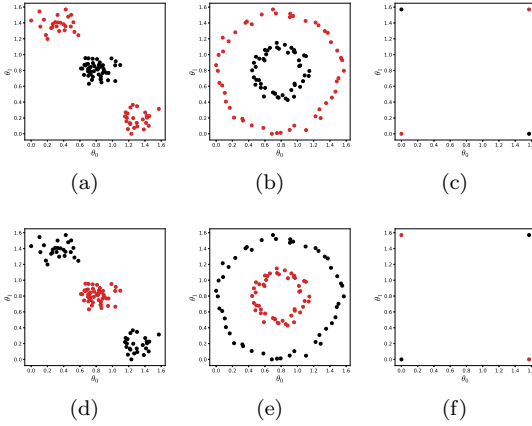


Figure 7: Classification problems where the quantum neurons are applied in this work. The positive class is represented by the black blobs, while the negative class is represented by the red ones. All inputs are in the interval  $[0, \pi/2]$ .

## 5.1 Datasets

The three datasets used in this work are depicted in Figure 7a, Figure 7b, and Figure 7c. Here, the positive class is represented by the black blobs, while the negative class is represented by the red blobs, although there is no previous indication of that labeling. Thus, we decide to swap the labels, deriving three more classification problems where the old negative classes become the new positive classes and vice versa, as depicted in Figure 7d, Figure 7e, and Figure 7f. Note that a line is not able to separate the classes of any of those two-dimensional binary classification problems. It is worth also mentioning that each input variable is scaled to that interval  $[0, \pi/2]$ .

We refer to Figure 7a and Figure 7d as the diagonal blobs due to the formed structure. The difference is that the target is the center blobs in Figure 7a, while the target is the corner blobs in Figure 7d. That dataset is provided by the scikit-learn *make\_blobs* function, letting *centers* be  $[(-5,8), (0,0), (5,-8)]$ , *cluster\_std* be 1.2, and *random\_state* be 0. Each class has 50 samples. Alternatively, the target

is the inner circle in Figure 7b, while the target is the outer circle in Figure 7e. Those concentric circles are provided by the scikit-learn *make\_circles* function, letting *noise* be 0.05, *factor* be 0.4, and *random\_state* be 0. Each circle has 50 samples. Finally, the blobs in the coordinates  $[(0, 0), (0, \pi/2), (\pi/2, 0), (\pi/2, \pi/2)]$  form a square, where the target is like the Exclusive OR (XOR) problem in Figure 7c, while the target is like the Not Exclusive OR (NXOR) problem in Figure 7f.

## 5.2 Search for Weights and Parameters

In this work, we conduct a grid search for the best weight vector of each quantum neuron for each classification problem. The space of weight vectors is formed here by all vectors  $(\phi_0, \phi_1)$  where each component assumes one-hundred equidistant values in the interval  $[0, \pi/2]$ , which gives a ten-thousand-vector weight space. Then, we choose the first weight vector in the search that maximizes the Area Under the Receiver Operating Characteristic Curve (AUC ROC). The AUC ROC allows measuring the classification quality in a threshold-free manner. We compute that metric by means of the scikit-learn *roc\_auc\_score* function.

Specifically for the PCDQN, we conduct a nested grid search for the best parameter combination and weight vector for each classification problem. The space of parameters is formed here by all combinations  $(\tau, \delta)$ , where

$$\tau \in \left\{ \frac{1}{4}, \frac{1}{2}, 1, 2, 4 \right\}$$

and

$$\delta \in \left\{ 0, \frac{\pi}{4}, \frac{\pi}{2}, \frac{3\pi}{4}, \pi, \frac{5\pi}{4}, \frac{3\pi}{2} \right\}.$$

Actually, the combination  $(1, 0)$  is not allowed since it produces the CDQN. Consequently, there are 34 allowed combinations to search. Those combinations explore a variety of lengths and shifts along the activation function period, which

is  $2\pi$ . For each combination of  $\tau$  and  $\delta$ , we search that ten-thousand-vector weight space. Then, we choose the first values of  $(\tau, \delta)$  and  $(\phi_0, \phi_1)$  that maximize the AUC ROC together in the nested search.

### 5.3 Results and Discussion

Table 1 shows the maximum AUC ROC that each quantum neuron achieved for each classification problem. The CVQN and the CDQN perfectly solved the Diagonal blobs when targeting the class Center. The CVQN also solved the NXOR-like Square blobs, while the CDQN performed like a random model. On the other hand, while the CVQN did not solve the Concentric circles when targeting the class Inner, the CDQN did. In summary, the CVQN and the CDQN only solved two problems each. The PCDQN produced optimal solutions for all problems, even for those problems where the other neurons performed like merely random models. Those results confirm the hypothesis that parametrization gives flexibility.

The best parameter combinations and weight vectors of each quantum neuron for each classification problem are reported in Table 2. Actually, the weights have about sixteen decimal places. We report here only the first two decimal places, which is enough to retrieve the original weights.

In the following, we use those best parameters and weights to study the quantum neuron solutions. We then plot the activation shape of each quantum neuron for each classification problem, which depends on the best parameters for the PCDQN. Those shapes are drawn as functions of the Euclidean distance from the input data to the corresponding best weight vector. A problem is solved if the neuron outputs for the black blobs are higher than the ones for the red blobs, regardless of the Euclidean distances to the best weight vector. In this way, there will be a threshold that separates the classes perfectly.

Figure 8 contrasts the quantum neuron solutions for the two problems derived from the Diagonal blobs. The CVQN solves the problem

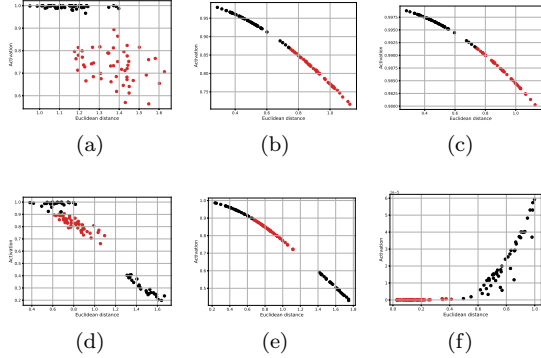


Figure 8: Solutions obtained by the CVQN, the CDQN, and the PCDQN, respectively, for the two problems derived from the Diagonal blobs. (a), (b), and (c) when targeting the class Center. (d), (e), and (f) when targeting the class Corner.

when targeting the class Center by positioning the weight vector closer to the center cluster, which gives values of activation for that cluster higher than the ones for the corner clusters, as shown in Figure 8a. That CVQN solution required the ability to also distinguish the black blobs from the red blobs at the intersection of Euclidean distances between the clusters. A similar CVQN solution correctly separated the upper left cluster from the center cluster when targeting the class Corner, although the bottom right cluster has incorrectly obtained the lowest values, as shown in Figure 8d. The CDQN and the PCDQN solve the problem when targeting the class Center by positioning the weight vector close to the target cluster, and then implementing a monotonic decay as the Euclidean distance increases in any direction, as shown in Figure 8b and Figure 8c. A monotonic decay does not solve the problem when targeting the class Corner, as shown in Figure 8e for the CDQN. Actually, a monotonic growth from a weight vector within the center cluster solves that problem, as shown in Figure 8f for the PCDQN, which can be achieved by means of parametrization.

The quantum neuron solutions for the two problems derived from the Concentric circles are

Table 1: Maximum AUC ROC of Each Quantum Neuron for Each Classification Problem.

Dataset	Target	CVQN	CDQN	PCDQN
Diagonal blobs	Center	<b>1.0</b>	<b>1.0</b>	<b>1.0</b>
	Corner	0.5	0.5	<b>1.0</b>
Concentric circles	Inner	0.8244	<b>1.0</b>	<b>1.0</b>
	Outer	0.502	0.4088	<b>0.9524</b>
Square blobs	XOR-like	0.5	0.5	<b>1.0</b>
	NXOR-like	<b>1.0</b>	0.5	<b>1.0</b>

Table 2: Best Parameter Combinations and Weight Vectors of Each Quantum Neuron for Each Classification Problem.

Dataset	Target	CVQN	CDQN	PCDQN	
		$(\phi_0, \phi_1)$	$(\phi_0, \phi_1)$	$(\tau, \delta)$	$(\phi_0, \phi_1)$
Diagonal blobs	Center	(0, 0)	(0.46, 0.49)	(1/4, 0)	(0.46, 0.50)
	Corner	(0, 0.87)	(0, 1.07)	(1/4, $\pi$ )	(0.69, 0.76)
Concentric circles	Inner	(0, 0.03)	(0.60, 0.76)	(1/4, 0)	(0.60, 0.76)
	Outer	(0.79, 0)	(1.57, 1.45)	(1/4, $\pi$ )	(0.82, 0.74)
Square blobs	XOR-like	(0, 0.79)	(0, 0)	(4, 0)	(0.15, 1.20)
	NXOR-like	(0, 0)	(0, 0)	(4, 0)	(0.04, 0.04)

contrasted in Figure 9. The CVQN correctly separates the classes at the intersection of Euclidean distances between them when targeting the class Inner, as shown in Figure 9a. The CVQN does not solve the problem because the closest and the most distant blobs, which are of the negative class, obtained high values of activation. Figure 9d shows that the CVQN performed like a random model when targeting the class Outer because the solution basically implements a decay. However, the circle shapes inside that solution suggest the multiple neuron outputs for the same Euclidean distance depend on the distance direction. The CDQN and the PCDQN solve the problem when targeting the class Inner by implementing a monotonic decay from that target circle, as shown in Figure 9b and Figure 9c. That shape does not fit the problem when targeting the class Outer, as shown in Figure 9e for the CDQN. A monotonic growth from the center can really fit that problem, which can be achieved by parametrization, as shown in Figure 9f for the PCDQN. That solution does not fit perfectly because far blobs obtained low val-

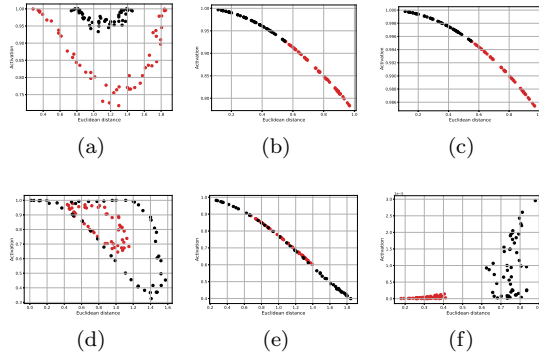


Figure 9: Solutions obtained by the CVQN, the CDQN, and the PCDQN, respectively, for the two problems derived from the Concentric circles. (a), (b), and (c) when targeting the class Inner. (d), (e), and (f) when targeting the class Outer.

ues of activation. Thus, the distance direction really matters.

Finally, Figure 10 contrasts the quantum neu-

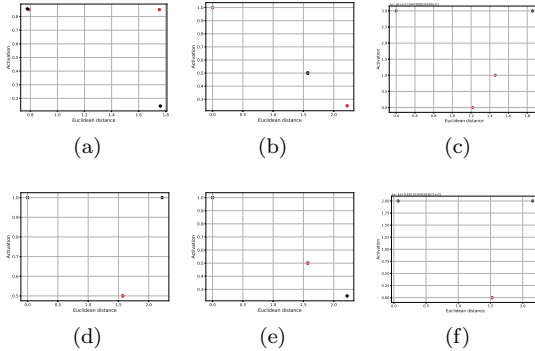


Figure 10: Solutions obtained by the CVQN, the CDQN, and the PCDQN, respectively, for the two problems derived from the Square blobs. (a), (b), and (c) when targeting the XOR problem. (d), (e), and (f) when targeting the NXOR problem.

ron solutions for the two problems derived from the Square blobs. The CVQN performed as a random model when targeting the XOR-like problem because the solution basically implements a decay, as shown in Figure 10a. A distant point obtained a high value of activation due to its distance direction. The CVQN solves the problem perfectly when targeting the NXOR-like problem by taking advantage of all spectrum of its activation shape to generate high values of activation in the extremes and low values in the intermediate distances, as shown in Figure 10d. A monotonic decay does not fit any of those two problems, as shown in Figure 10b and Figure 10e, both for the CDQN. In contrast, a concave-up parabola can fit those two problems. By the way, the PCDQN can implement such shape, as already shown in Figure 6f. Thus, the PCDQN can solve those two problems perfectly, as shown in Figure 10c and Figure 10f.

Those results demonstrate limitations in the CVQN and in the CDQN since their activation shapes can fit only particular problems. The PCDQN, in turn, can dynamically change its activation shape to a monotonic decay, a monotonic growth, and a concave-up parabola, for ex-

ample. That list of shapes is not exhaustive. The PCDQN can implement even more shapes by exploring its real parameters, depending on the underlying pattern of the problem. Thus, the PCDQN is flexible. Such flexibility allows the PCDQN to fit complex problems that are beyond the capabilities of the other neurons.

## 5.4 Execution on a Quantum Simulator

Finally, we demonstrate the physical feasibility of the previous numerical solutions through a proof-of-concept experiment on a quantum simulator. We address here the two classification problems used in [13]: Diagonal blobs targeting the class Center and Concentric circles targeting the class Inner. The quantum neuron solutions for those two problems are then implemented in quantum circuits that are executed on the Qiskit QASM simulator.

To estimate the quantum neuron activation for a given pair of vectors, we take the proportion of 1's in the circuit outputs after twenty thousand executions of the circuit. Thus, each quantum neuron is executed twenty thousand times for each input vector of each classification problem to estimate the activation with respect to the corresponding best weight vector. Twenty thousand executions of three quantum neurons applied in two classification problems of a hundred samples each give twelve million circuit executions. Nevertheless, finite numbers of execution can cause small errors in the activation estimates.

After estimating the activation, we can compute the circuit-generated AUC ROC of each quantum neuron for each classification problem on the quantum simulator. Those circuit-generated values of AUC ROC are contrasted in Figure 11. The blue bars represent the CVQN, the orange bars represent the CDQN, and the green bars represent the PCDQN. In fact, the quantum neurons reproduce the reference values reported in Table 1 for those two problems. The CDQN and the PCDQN generate optimal

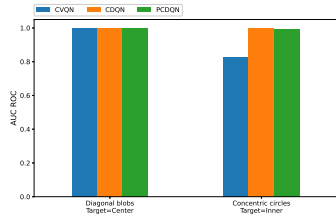


Figure 11: AUC ROC generated by the quantum neuron circuits on a quantum simulator for the Diagonal blobs when targeting the class Center and the Concentric circles when targeting the class Inner. The blue, orange, and green bars represent the CVQN, the CDQN, and the PCDQN, respectively.

results, while the CVQN is optimal in the first problem but generates an AUC ROC of about 0.82 in the second problem. Therefore, the quantum neuron solutions are validated by the circuit realizations in the quantum simulator.

## 6 Conclusions

In this paper, we proposed a generalized framework to build quantum neurons that apply the kernel trick. We highlight that the feature space mapping is what determines each quantum neuron under the proposed framework. Each particular case only instantiates the transformation that is applied to the input and weight vectors. It makes room to define countless quantum neurons, including for actual quantum devices, as long as the feature mappings can be implemented in quantum circuits. Feature mappings hard to compute classically may solve practical problems more efficiently, which will represent a quantum advantage achieved by that quantum neuron framework.

Under that framework, we presented a quantum neuron with a parametrized activation function and an efficient circuit implementation. That circuit implementation further complies with the constraints of actual quantum devices compared to the existing neuron. Firstly, a cir-

cuit with constant depth and a linear number of operations mitigates the errors by decoherence times and gate infidelities. Qubit encoding generates a straightforward state preparation. Connectivity is not a problem since that encoding strategy generates separable states. Circuit rewriting is facilitated since the circuit uses elementary single-qubit gates. Additionally, the proposed neuron is still flexible due to the parametrization of its activation function.

Each quantum neuron implements a fundamentally different activation function. Here, we showed the neuron activation shapes as functions of some relations between the input and weight vectors. While the existing neuron is restricted, the parametrized neuron can fit different problem structures. As a demonstration, the parametrized neuron produced optimal solutions for the six classification problems addressed here, while the existing neuron only solved two problems. The proposed neuron without parametrization also solved only two problems. Thus, parametrizing really improves the neuron capabilities. Finally, we also demonstrated that the quantum neuron circuits can reproduce the numerical solutions.

Future works can discover other quantum neurons under the proposed framework by using other gates, combining gates, applying heterogeneous gates, or even evolving some evolutionary approach to learn the optimal feature mapping for a classification problem. A theoretical study can define the bounds of that framework or even prove that it is universal. Subsequent works can extend the comparison between the quantum neurons to other classification problems executed also on real quantum devices. As an alternative, weights and parameters can be adjusted by variational quantum algorithms [38, 39]. Finally, a network of quantum neurons under the proposed framework can be constructed.

## Acknowledgments

This work was supported by the Foundation for the Support of Science and Technology of the

State of Pernambuco (Fundação de Amparo à Ciência e Tecnologia do Estado de Pernambuco - FACEPE) under Grant Number IBPG-0084-1.03/20 and Grant Number APQ-1110-1.03/21.

## References

- [1] M. A. Nielsen and I. L. Chuang, *Quantum Computation and Quantum Information*. New York, USA: Cambridge University Press, 2010.
- [2] J. Preskill, “Quantum computing and the entanglement frontier,” *arXiv preprint arXiv:1203.5813*, 2012.
- [3] N. H. Nguyen, E. C. Behrman, M. A. Moustafa, and J. E. Steck, “Benchmarking neural networks for quantum computations,” *IEEE Transactions on Neural Networks and Learning Systems*, vol. 31, no. 7, pp. 2522–2531, 2020.
- [4] F. M. de Paula Neto, T. B. Ludermir, W. R. de Oliveira, and A. J. da Silva, “Implementing any nonlinear quantum neuron,” *IEEE Transactions on Neural Networks and Learning Systems*, vol. 31, no. 9, pp. 3741–3746, 2020.
- [5] S. J. Devitt, W. J. Munro, and K. Nemoto, “Quantum error correction for beginners,” *Reports on Progress in Physics*, vol. 76, no. 7, p. 076001, 2013.
- [6] J. Preskill, “Quantum computing in the nisq era and beyond,” *Quantum*, vol. 2, p. 79, 2018.
- [7] F. Leymann and J. Barzen, “The bitter truth about gate-based quantum algorithms in the nisq era,” *Quantum Science and Technology*, vol. 5, no. 4, p. 044007, 2020.
- [8] A. Zulehner, A. Paler, and R. Wille, “An efficient methodology for mapping quantum circuits to the ibm qx architectures,” *IEEE Transactions on Computer-Aided Design of Integrated Circuits and Systems*, vol. 38, no. 7, pp. 1226–1236, 2019.
- [9] R. LaRose, “Overview and comparison of gate level quantum software platforms,” *Quantum*, vol. 3, p. 130, 2019.
- [10] F. Acasiete, F. P. Agostini, J. K. Moqadam, and R. Portugal, “Implementation of quantum walks on ibm quantum computers,” *Quantum Information Processing*, vol. 19, no. 426, 2020.
- [11] G. Acampora and A. Vitiello, “Implementing evolutionary optimization on actual quantum processors,” *Information Sciences*, vol. 575, pp. 542–562, 2021.
- [12] F. Tacchino, C. Macchiavello, D. Gerace, and D. Bajoni, “An artificial neuron implemented on an actual quantum processor,” *npj Quantum Information*, vol. 5, no. 26, 2019.
- [13] S. Mangini, F. Tacchino, D. Gerace, C. Macchiavello, and D. Bajoni, “Quantum computing model of an artificial neuron with continuously valued input data,” *Machine Learning: Science and Technology*, vol. 1, no. 045008, 2020.
- [14] F. Tacchino, P. Barkoutsos, C. Macchiavello, I. Tavernelli, D. Gerace, and D. Bajoni, “Quantum implementation of an artificial feed-forward neural network,” *Quantum Science and Technology*, vol. 5, no. 4, p. 044010, 2020.
- [15] E. Grant, M. Benedetti, S. Cao, A. Hallam, J. Lockhart, V. Stojevic, A. G. Green, and S. Severini, “Hierarchical quantum classifiers,” *npj Quantum Information*, vol. 4, no. 65, 2018.
- [16] I. Cong, S. Choi, and M. D. Lukin, “Quantum convolutional neural networks,” *Nature Physics*, vol. 15, pp. 1273–1278, 2019.



- [17] P.-L. Dallaire-Demers and N. Killoran, “Quantum generative adversarial networks,” *Physical Review A*, vol. 98, no. 1, p. 012324, 2018.
- [18] C. Zoufal, A. Lucchi, and S. Woerner, “Quantum generative adversarial networks for learning and loading random distributions,” *npj Quantum Information*, vol. 5, no. 103, 2019.
- [19] D. Konar, S. Bhattacharyya, B. K. Panigrahi, and E. C. Behrman, “Qutrit-inspired fully self-supervised shallow quantum learning network for brain tumor segmentation,” *IEEE Transactions on Neural Networks and Learning Systems*, 2021. early access.
- [20] H. Buhrman, R. Cleve, J. Watrous, and R. de Wolf, “Quantum fingerprinting,” *Physical Review Letters*, vol. 87, no. 16, p. 167902, 2001.
- [21] V. Havlíček, A. D. Córcoles, K. Temme, A. W. Harrow, A. Kandala, J. M. Chow, and J. M. Gambetta, “Supervised learning with quantum-enhanced feature spaces,” *Nature*, vol. 567, pp. 209–212, 2019.
- [22] M. Schuld and N. Killoran, “Quantum machine learning in feature hilbert spaces,” *Physical Review Letters*, vol. 122, no. 4, p. 040504, 2019.
- [23] C. Ding, T.-Y. Bao, and H.-L. Huang, “Quantum-inspired support vector machine,” *IEEE Transactions on Neural Networks and Learning Systems*, 2021. early access.
- [24] Y. Liu, S. Arunachalam, and K. Temme, “A rigorous and robust quantum speed-up in supervised machine learning,” *Nature Physics*, vol. 17, pp. 1013–1017, 2021.
- [25] S. Bravyi, D. Gosset, and R. König, “Quantum advantage with shallow circuits,” *Science*, vol. 362, no. 6412, pp. 308–311, 2018.
- [26] S. Bravyi, D. Gosset, R. König, and M. Tomamichel, “Quantum advantage with noisy shallow circuits,” *Nature Physics*, vol. 16, pp. 1040–1045, 2020.
- [27] Y. Li and S. C. Benjamin, “Efficient variational quantum simulator incorporating active error minimization,” *Physical Review X*, vol. 7, no. 021050, 2017.
- [28] K. Temme, S. Bravyi, and J. M. Gambetta, “Error mitigation for short-depth quantum circuits,” *Physical Review Letters*, vol. 119, no. 180509, 2017.
- [29] A. Kandala, K. Temme, A. D. Córcoles, A. Mezzacapo, J. M. Chow, and J. M. Gambetta, “Error mitigation extends the computational reach of a noisy quantum processor,” *Nature*, vol. 567, pp. 491–495, 2019.
- [30] E. M. Stoudenmire and D. J. Schwab, “Supervised learning with tensor networks,” in *Advances in Neural Information Processing Systems (NeurIPS Proceedings)* (D. Lee, M. Sugiyama, U. Luxburg, I. Guyon, and R. Garnett, eds.), vol. 29, Curran Associates, Inc., 2016.
- [31] T. M. Cover, “Geometrical and statistical properties of systems of linear inequalities with applications in pattern recognition,” *IEEE Transactions on Electronic Computers*, vol. EC-14, no. 3, pp. 326–334, 1965.
- [32] N. S. Yanofsky and M. A. Mannucci, *Quantum Computing for Computer Scientists*. New York, USA: Cambridge University Press, 2008.
- [33] S. Haykin, *Neural Networks and Learning Machines*. New Jersey, USA: Pearson, 2009.
- [34] C. M. Bishop, *Pattern Recognition and Machine Learning*. New York, USA: Springer, 2006.
- [35] M. Rossi, M. Huber, D. Bruß, and C. Macchiavello, “Quantum hypergraph states,”



*New Journal of Physics*, vol. 15, no. 113022, 2013.

- [36] M. S. Anis, Abby-Mitchell, H. Abraham, AduOffei, R. Agarwal, G. Agliardi, M. Aharoni, I. Y. Akhalwaya, G. Aleksandrowicz, T. Alexander, M. Amy, S. Anagolum, *et al.*, “Qiskit: An open-source framework for quantum computing,” 2021.
- [37] F. Pedregosa, G. Varoquaux, A. Gramfort, V. Michel, B. Thirion, O. Grisel, M. Blondel, P. Prettenhofer, R. Weiss, V. Dubourg, J. Vanderplas, A. Passos, *et al.*, “Scikit-learn: Machine learning in python,” *Journal of Machine Learning Research*, vol. 12, no. 85, pp. 2825–2830, 2011.
- [38] M. Cerezo, A. Arrasmith, R. Babbush, S. C. Benjamin, S. Endo, K. Fujii, J. R. McClean, K. Mitarai, X. Yuan, L. Cincio, and P. J. Coles, “Variational quantum algorithms,” *Nature Reviews Physics*, vol. 3, pp. 625–644, 2021.
- [39] R. Huang, X. Tan, and Q. Xu, “Learning to learn variational quantum algorithm,” *IEEE Transactions on Neural Networks and Learning Systems*, 2022. early access.